



Inlet Development for a Rocket Based Combined Cycle, Single Stage to Orbit Vehicle Using Computational Fluid Dynamics

J.R. DeBonis, C.J. Trefny, and C.J. Steffen, Jr.
Glenn Research Center, Cleveland, Ohio

The NASA STI Program Office . . . in Profile

Since its founding, NASA has been dedicated to the advancement of aeronautics and space science. The NASA Scientific and Technical Information (STI) Program Office plays a key part in helping NASA maintain this important role.

The NASA STI Program Office is operated by Langley Research Center, the Lead Center for NASA's scientific and technical information. The NASA STI Program Office provides access to the NASA STI Database, the largest collection of aeronautical and space science STI in the world. The Program Office is also NASA's institutional mechanism for disseminating the results of its research and development activities. These results are published by NASA in the NASA STI Report Series, which includes the following report types:

- **TECHNICAL PUBLICATION.** Reports of completed research or a major significant phase of research that present the results of NASA programs and include extensive data or theoretical analysis. Includes compilations of significant scientific and technical data and information deemed to be of continuing reference value. NASA's counterpart of peer-reviewed formal professional papers but has less stringent limitations on manuscript length and extent of graphic presentations.
- **TECHNICAL MEMORANDUM.** Scientific and technical findings that are preliminary or of specialized interest, e.g., quick release reports, working papers, and bibliographies that contain minimal annotation. Does not contain extensive analysis.
- **CONTRACTOR REPORT.** Scientific and technical findings by NASA-sponsored contractors and grantees.

- **CONFERENCE PUBLICATION.** Collected papers from scientific and technical conferences, symposia, seminars, or other meetings sponsored or cosponsored by NASA.
- **SPECIAL PUBLICATION.** Scientific, technical, or historical information from NASA programs, projects, and missions, often concerned with subjects having substantial public interest.
- **TECHNICAL TRANSLATION.** English-language translations of foreign scientific and technical material pertinent to NASA's mission.

Specialized services that complement the STI Program Office's diverse offerings include creating custom thesauri, building customized data bases, organizing and publishing research results . . . even providing videos.

For more information about the NASA STI Program Office, see the following:

- Access the NASA STI Program Home Page at <http://www.sti.nasa.gov>
- E-mail your question via the Internet to help@sti.nasa.gov
- Fax your question to the NASA Access Help Desk at (301) 621-0134
- Telephone the NASA Access Help Desk at (301) 621-0390
- Write to:
NASA Access Help Desk
NASA Center for Aerospace Information
7121 Standard Drive
Hanover, MD 21076



Inlet Development for a Rocket Based Combined Cycle, Single Stage to Orbit Vehicle Using Computational Fluid Dynamics

J.R. DeBonis, C.J. Trefny, and C.J. Steffen, Jr.
Glenn Research Center, Cleveland, Ohio

Prepared for the
35th Joint Propulsion Conference and Exhibit
cosponsored by the AIAA, ASME, SAE, and ASEE
Los Angeles, California, June 20-24, 1999

National Aeronautics and
Space Administration

Glenn Research Center

Available from

NASA Center for Aerospace Information
7121 Standard Drive
Hanover, MD 21076
Price Code: A03

National Technical Information Service
5285 Port Royal Road
Springfield, VA 22100
Price Code: A03

INLET DEVELOPMENT FOR A ROCKET BASED COMBINED CYCLE, SINGLE STAGE TO ORBIT VEHICLE USING COMPUTATIONAL FLUID DYNAMICS

James R. DeBonis*, Charles J. Trefny†, and Christopher J. Steffen Jr.†
 NASA Glenn Research Center
 Cleveland, Ohio 44135

Abstract

Design and analysis of the inlet for a rocket based combined cycle engine is discussed. Computational fluid dynamics was used in both the design and subsequent analysis. Reynolds averaged Navier-Stokes simulations were performed using both perfect gas and real gas assumptions. An inlet design that operates over the required Mach number range from 0 to 12 was produced. Performance data for cycle analysis was post processed using a stream thrust averaging technique. A detailed performance database for cycle analysis is presented. The effect of vehicle forebody compression on air capture is also examined.

Nomenclature

A	cross sectional area
D	drag
F	stream thrust
H	total enthalpy
M	Mach number
Q	dynamic pressure
R	gas constant
U	one-dimensional velocity
\vec{V}	velocity vector
c_p	specific heat at constant pressure
\vec{f}	flow direction unit vector
h	enthalpy
\dot{m}	massflow
p	pressure
r	radius
x	distance from station 3
ρ	density

subscripts

0	station 0, freestream
1	station 1
2	station 2
3	station 3
b	body
c	capture
cl	cowl
cb	centerbody
d	diverter
t	total condition

superscripts

-	stream thrust averaged quantity
---	---------------------------------

Introduction

One of the three primary goals of NASA's Aeronautics and Space Transportation Technology program is to enable low cost access to space by developing advanced space transportation concepts and technologies. The key to reducing space launch costs is developing a reusable vehicle with a short turn-around time. Highly reusable implies a very robust Single-Stage-to-Orbit (SSTO) vehicle. NASA's Glenn Research Center has undertaken a program to demonstrate such a vehicle. The concept, called the Trailblazer¹ (figure 1), is powered by a Rocket Based Combined Cycle (RBCC) engine (figure 2). This engine is designed to operate efficiently from lift-off to orbit by integrating a rocket and ramjet². The system combines the high thrust-to-weight/low specific impulse characteristics of the rocket with the high specific impulse/low thrust to weight characteristics of the ramjet. The engine operates in air-breathing modes from lift-off to between Mach 10 and 12, at which point the airbreathing engine flow path is closed off, and the rocket is turned back on to carry the vehicle out of the atmosphere and into orbit. Three semi-circular engine pods are located near the aft portion of the vehicle. The pods allow for diversion of the boundary layer, simplify centerbody actuation and sealing, and enable integration of the nozzles with the vehicle base.

* Aerospace Engineer, Nozzle Branch, Senior Member AIAA

† Aerospace Engineer, Engine Systems Technology Branch, Senior Member AIAA

An important component of the RBCC engine is the inlet. This device must efficiently capture and compress the air over the entire range of air-breathing Mach numbers. The objective of this work was to design an inlet and provide detailed performance data for engine cycle analysis. Computational fluid dynamics (CFD) was used in both the design and analysis process. CFD provided a fast and efficient method for obtaining high fidelity performance data for the Trailblazer design effort.

Inlet Design

Traditional design methods involve point designs at a cruise condition and are not applicable to this problem. The resulting inlets have very good cruise performance but may suffer at off-design conditions. Inlets for airbreathing SSTO vehicles must trade high efficiency at one Mach number for good performance over the entire Mach range. Weight and wetted area must also be considered. Several design decisions were initially made to guide the process. A mixed compression inlet with a translating centerbody was chosen. Moving the centerbody allows the inlet to start and varies the contraction ratio over the Mach number range. For rocket only operation (in vacuum conditions), the inlet duct must be completely closed off. The inlet duct was designed to accomplish this by fully retracting the centerbody. The inlet is intended to operate without boundary layer bleed to keep the system weight to a minimum and maintain simplicity.

The key locations for cycle analysis are indicated in figure 2. Station 0 is the freestream. Station 1 is located at the inlet spike tip. Station 2 is the inlet throat and is used as the nominal location for the beginning of supersonic combustion/fuel injection. Station 3 is at the end of a fixed hub over which the centerbody translates. The inlet geometry and key design parameters are shown in figure 3. The cowl lip radius is used to size the inlet. The maximum radius of the centerbody was chosen so that the annular area formed by the cowl lip and centerbody is equal to the area at station 3. A 12-degree cone angle was chosen to minimize length. At station 2, the inlet throat is angled at 15 degrees towards the axis to minimize length and wetted area in the diffuser/scram combustor portion of the flowpath. A back step in the centerbody is placed here to isolate the forward portion of the inlet from back pressure feeding forward through the subsonic portion of the boundary layer and can serve as a location for fuel injectors. A constant area section to facilitate scramjet ignition is located aft of the step. The angle at the end of the centerbody is specified at 20 degrees. A flat section is located on the forward

portion of the cowl to allow the inlet to be oversped (shock inside the lip).

Isentropic inlet contours for Mach 6 operation were generated using a method of characteristics design code³ based on the aforementioned constraints. Mach 6 was chosen as the key point in the flight envelope. Beyond this point, the required inlet contraction ratio does not change appreciably with Mach number. Centerbody shock on lip was specified at this Mach number and the shoulder on the centerbody was placed to cancel the reflected cowl shock. Beyond Mach 6, the shock angle does not change significantly with increased Mach number due to the hypersonic Mach number independence principle. Thus, the reflected shock will remain near the shoulder for all hypersonic Mach numbers.

Several perfect gas CFD analyses using the NPARC code were done on preliminary configurations. The CFD solutions were used to evaluate the designs and provide guidance in adjusting the key geometric parameters. In particular, predictions of shock strength and location, potential boundary layer separations, and throat Mach number were used to adjust the inlet lines. The final inlet geometry is completely described in table 1.

CFD Method

The flowfield was assumed to be axisymmetric so that two-dimensional CFD could be used. This assumption is valid for a large majority of the inlet flow. Only the effects of the inlet sidewalls/endwalls would alter the flowfield in the circumferential direction. The assumption significantly reduces the number of grid points required to describe the geometry and hence reduces the computational cost for a solution. Two-dimensional CFD yielded timely results for the inlet design process and enabled a large number of cases to be run for cycle analysis. Solid walls were specified with an adiabatic no-slip wall boundary condition.

Grid Generation

The inlet geometry is defined by a series of cubic splines and other simple geometric shapes. The spline data was used to create a series of points on the inlet surface that were read into the grid generator.

The grid generation software used for this project was GRIDGEN⁴. It is an interactive software package with a user-friendly graphical interface. It is capable of producing high quality structured and unstructured grids for complex two and three-dimensional geometries.

All grids were generated such that the first grid point away from a viscous wall was placed at an average inner variable distance, y^+ , of 1. This distance was computed based on assumed average skin friction and flowfield values, and was subsequently checked for accuracy. It has been shown that proper resolution of the boundary layer is not possible unless at least one grid point is within a y^+ of two⁵.

A typical grid is shown in figure 4. The grid uses a blocked structure with point-to-point matching at the block interfaces. For started supersonic cases, it was not necessary to model the area above the cowl lip because the flow in this region does not influence the region of interest and is not captured by the inlet. Thus, the grid above the cowl lip was not used for these cases. A grid sensitivity study was performed with the GASP code. Doubling the number of grid points in each direction did not significantly affect the solution.

NPARC

The NPARC code⁶ was used for the perfect gas analyses. NPARC is developed and supported by the NPARC Alliance, a collaboration between the NASA Glenn Research Center and the United States Air Force's Arnold Engineering Development Center. NPARC solves the Reynolds averaged Navier-Stokes equations in strong conservation law form using the Beam-Warming approximate factorizations algorithm⁷. Spatial discretization is performed using a central difference scheme. Jameson style artificial dissipation⁸ is added for stability and to smooth shock oscillations and odd-even grid point decoupling. The code uses a perfect gas equation of state. The code has several options for modeling turbulence varying from algebraic zero transport equations to one and two equation models. Both the Chien low Reynolds number $k-\epsilon$ ⁹ and Wilcox's $k-\omega$ ¹⁰ models were investigated for this work. It was found that the two-equation models produce very similar answers. All data reported from the NPARC code was generated using the $k-\epsilon$ model.

GASP

The GASP code¹¹ was used for the real gas analyses. GASP is a commercially available code that is developed and sold by Aerosoft Inc. For this analysis the code solved the Reynolds averaged Navier-Stokes equations using a third-order accurate upwind scheme and Roe's flux difference splitting¹². Time discretization was done by a two-factor alternating direction implicit (ADI) scheme. Van Albada limiters¹³ were employed for stability in the presence of discontinuities. The chemical kinetics model of Kang

et. al.¹⁴ was used. The equilibrium vibrational thermodynamics model was selected. The $k-\omega$ turbulence model was found most robust and was used for all GASP results herein. To ensure that there were no discrepancies between codes due to the difference in turbulence models, both NPARC with the $k-\epsilon$ model and GASP with the $k-\omega$ were run using the perfect gas assumption at several Mach numbers. Integrated results agreed within one percent for all Mach numbers except Mach 6, where the difference was approximately 5 percent in total pressure recovery and 2 percent in Mach number.

Inlet Performance Analysis

Results were obtained for freestream Mach numbers from 0.5 to 12. The corresponding station 1 Mach numbers, used for the inflow boundary condition, were derived based on a 10-degree conical shock and re-expansion to freestream pressure (table 2). A subsequent two-dimensional analysis of the vehicle forebody provided more accurate results and is discussed in a later section. For the subsonic cases (Mach 0.5 and 0.8), the centerbody was completely extended and the mass flux on the outflow boundary was regulated to control the inlet flow. For supersonic cases up to Mach 6 (the transition Mach number from subsonic to supersonic combustion), several supercritical (no back pressure imposed) cases were run to determine a centerbody position which provided the maximum contraction ratio. Then using this centerbody position, a back pressure was applied through the exit boundary condition to simulate the effect of the combustion process. This back pressure was increased in several increments until the inlet was unstalled. The data at maximum back pressure is presented here. Beyond Mach 6, only super-critical cases were necessary due to the supersonic combustion process. Three inlet contraction ratios were run at these Mach numbers to provide a range of data (figure 5). Billig's suggested contraction ratio¹⁵ is shown for comparison. The maximum contraction ratio was found to be about 16 for all hypersonic Mach numbers (Mach 6 and above). Results using the perfect gas code (NPARC) were run at all Mach numbers. Real gas results (GASP) were obtained for Mach 4 and higher.

Representative Mach number contours, from the NPARC code, are shown in figure 6 for Mach 0.8, Mach 2, and Mach 6 (started) operation. A mildly supercritical solution is presented for Mach 0.8. Choking at the centerbody shoulder determines the maximum airflow. A normal shock is located just downstream. The plot also shows a region of low pressure on the cowl, which creates a suction force.

At Mach 2, a classical lambda-shock pattern appears just forward of the cowl lip. This case is slightly sub-critical, 10 percent more airflow was observed at very low back pressure. The shock induced separation reduces the flow area and the flow chokes at the aerodynamic throat. The Mach 6 contours show shock-on-lip operation. It is evident that the cowl shock is not completely canceled on the forebody at this Mach number. Viscous effects were not accounted for in the MOC design code and alter the Mach number at which the shock is canceled. Because the inlet is not a point design, the exact Mach number where the shock is canceled is not significant. For all started cases the cowl shock wave strikes the centerbody shoulder and the resulting pressure gradient separates the boundary layer. This separation is the dominant mechanism in the flowfield. Centerbody surface static pressure distributions for Mach 6 are presented in figure 7. Several back pressured cases, super-critical to maximum back pressure ($350p_0$), are shown.

Stream Thrust Averaging

An averaging procedure which conserves mass, momentum and energy was used to compute integrated one-dimensional performance data from the two-dimensional CFD solutions. This stream thrust averaging (STA) technique provides a consistent set of data for use in cycle analysis. In STA the distorted 2-D profile is passed through an idealized control volume where the flow is completely mixed at the exit. The equations are derived by applying mass, momentum, and energy conservation to this process. The STA technique for a perfect gas is presented. To simplify the procedure, a unit vector in the flow direction, \vec{f} , is chosen based on the geometry. Then, for each plane of two-dimensional data the following integrations are performed.

Stream thrust,

$$F = \int_A (\rho \vec{V} \cdot d\vec{A}) \vec{V} \cdot \vec{f} + \int_A p d\vec{A} \cdot \vec{f}$$

Massflow,

$$\dot{m} = \int_A \rho \vec{V} \cdot d\vec{A}$$

Stagnation enthalpy,

$$H = \frac{1}{\dot{m}} \int_A (\rho \vec{V} \cdot d\vec{A}) \left(h + \frac{|\vec{V}|^2}{2} \right)$$

These three quantities are substituted into the following quadratic equation that is solved for the stream thrust averaged velocity, \bar{U} .

$$\bar{U}^2 \left(1 - \frac{R}{2c_p} \right) - \frac{F}{\dot{m}} \bar{U} + \frac{HR}{c_p} = 0$$

Selecting between two resulting solutions for \bar{U} is done by applying the second law of thermodynamics. The remaining variables can then be found as follows.

$$\bar{p} = \frac{\dot{m}}{\bar{U}A}, \quad \bar{p} = \frac{F}{A} - \bar{p}\bar{U}^2, \quad \bar{h} = \frac{c_p \bar{p}}{\bar{\rho}R}$$

A similar technique for the chemically reacting flow solutions was used.¹⁶

Mass Capture

Inlet mass capture versus station 1 Mach number is plotted in terms of the area ratio A_1/A_c in figure 8. Subsonic, supersonic external compression, and started regions are denoted by different symbols. The subsonic and external compression cases were run with a low back pressure specified at the outflow boundary to determine the maximum airflow possible. Sub-critical cases were run by specifying a lower mass flux at the outflow boundary. The inlet starts between Mach 2 and 2.5 and the shock-on-lip condition occurs at Mach 6. The lines connect the critical (maximum) airflow points.

Recovery

Stream thrust averaged total pressure recovery is presented in figure 9. For the perfect gas solutions, isentropic perfect gas relations were applied to the stream thrust averaged pressure and Mach number to obtain the stagnation condition. The reference stagnation condition, at station 1, was also obtained from isentropic relations. For the real gas solutions, the equilibrium air stagnation condition was determined from the stream thrust averaged state using the HAP code.¹⁷ The stagnation condition of the reference state, station 1, was also calculated this way. Recovery was independent of massflow for the subsonic and supersonic external compression cases. Between Mach 4 and 6 the combustion process transitions between subsonic and supersonic combustion modes so recoveries at both stations 2 and 3 are presented. Both perfect gas and real gas station 2 recoveries are shown. Mil. E-5007D is shown for comparison. The spike positions corresponding the recovery data are presented in table 2.

Inlet Drag

In the Trailblazer force accounting system, inlet drag consists of the force on the forward facing cowl surface and the additive drag due to spillage. The cowl force is computed by simply integrating the pressure and shear stress over the surface area. Additive drag is defined as the pressure force exerted on the captured stream tube. It is computed by

applying the control volume pictured in figure 10 to the CFD solutions. Figure 11 shows the drag forces as a function of station 1 Mach number. Lines connect the critical airflow points. At subsonic flight conditions the cowl lip pressure is less than ambient and helps offset the additive drag. At these Mach numbers the drag is the lowest at the critical mass capture. For supersonic cases below Mach 2.5 (external compression), separation and choking just aft of the cowl lip forces the normal shock onto the forward portion of the centerbody and the additive drag is large. At Mach 2.5, the inlet starts and the additive drag is significantly reduced.

Comparison Between Real and Perfect Gas Solutions

Figure 12 compares real and perfect gas solutions at station 2. The percentage difference in the data between perfect and real gas solutions increases with Mach number. For recovery, good agreement is obtained up to Mach 6. At Mach 10, the perfect gas recovery is 30 percent higher than the real gas value. For throat Mach number, the real gas result is just over 10 percent higher than the perfect gas result at Mach 6 and increases to 20 percent at Mach 10.

Vehicle Forebody Precompression

The Trailblazer vehicle differs from many other SSTO and hypersonic vehicles in the fact that the vehicle forebody is not designed as a compression surface for the inlet. The Trailblazer design has chosen to trade the efficiency of forebody compression for the simplicity and higher structural and volumetric efficiency of an axisymmetric vehicle. It was assumed that the captured airflow was processed by the shock resulting from a 10-degree cone, then re-expanded to freestream pressure at station 1. A computational study was performed to check the validity of this assumption.

An axisymmetric perfect gas CFD analysis, using NPARC, was performed on the forebody at Mach 2, 4, 6, 8, 10, and 12. The grid contained 239 nodes in the axial direction and 245 nodes in the radial direction. Increasing the grid size in both directions by 50 percent did not significantly affect the solution. The axisymmetric solution yields flowfield variables as a function of radial distance, r , for a given x -location. For each axial location, the solution was then mapped onto the projected aerodynamic capture area of the inlet. This capture area is offset from the vehicle body to allow for the boundary layer diverter (figure 13). The boundary layer diverter radius, r_d , is 111 percent of the vehicle body radius, r_b . Stream thrust averaging of

the flowfield over this area was then performed. A plot of mass capture versus axial location is presented in figure 14. The increase in mass capture over that of a freestream inlet is attributed to forebody compression. This increase in mass capture is reduced asymptotically as station 1 is moved aft and the flow re-expands to nearer freestream pressure. The reduction in capture for the high Mach numbers at forward locations on the body is due to the forebody shock lying inside the projected capture area at station 1. When this occurs, a portion of the captured area is not yet compressed by the forebody shock. However, it is important to note that all the flow in the captured stream tube can still be compressed by the shock before entering the inlet. In other words, the forebody shock lies outside the cowl lip. The location of station 1 for the current Trailblazer configuration is represented by the vertical dashed line. Data comparing the effect of the forebody precompression to the original assumption of isentropic expansion back to freestream pressure are shown in figure 15. At Mach 10 the pressure is twice that of freestream. Mass capture is likewise affected. A 70 percent increase in mass capture is seen at Mach 10. As shown in figure 15c, the stream thrust averaged recovery is also increased due to curvature of the forebody shock. Stream thrust averaged station 1 Mach number plotted versus freestream Mach number in figure 15d shows a reduction in station 1 Mach number from the original assumption. Concomitant with these effects is a radial variation in flow properties from the diverter surface to the bow shock. The effect of this distortion on inlet performance and operability is currently unknown.

Conclusions

Two-dimensional computational fluid dynamics was used to design and analyze the inlet for the Trailblazer vehicle. The inlet is designed to operate from Mach 0 to 12 without boundary layer bleed. A maximum contraction ratio of 16 for all hypersonic Mach numbers was obtained. Both perfect and real gas assumptions were used in the CFD analyses. The perfect gas and real gas solutions were in agreement up to Mach 4 for averaged throat Mach number and up to Mach 6 for recovery. At Mach 10, the perfect gas solutions yield recoveries 30 percent too high and Mach numbers 20 percent too low. Mass capture, total pressure recovery and inlet drag are presented for the entire Mach range.

An analysis of the integration of the inlet with the vehicle forebody was also undertaken. The results indicate that the compression due to the vehicle forebody results in higher static pressure, mass capture

and recovery. At Mach 10 the station 1 mass capture is increased by 70 percent, the pressure is increased by a factor of 2, and the recovery is increased by 20 percent.

References

¹ Trefny, C.J., "An Air-Breathing Launch Vehicle Concept for Single-Stage-to-Orbit," AIAA Paper 99-2730, June 1999.

² Escher, W.J.D., "Synerjet for Earth/Orbit Propulsion: Revisiting the 1966 NASA/Marquardt Composite (Airbreathing/Rocket) Propulsion System Study," SAE Paper 851163, May 1985.

³ Anderson, B.H., "Design of Supersonic Inlets by a Computer Program Incorporating the Method of Characteristics," NASA TN D-4960, January 1969.

⁴ GridGen Version 13 Users Manual, Pointwise Inc., Bedford Texas, 1998

⁵ Georgiadis, N. J., Dudek, J.C., and Tierney, T.P., "Grid Resolution and Turbulent Inflow Boundary Condition Recommendations for NPARC Calculations", AIAA Paper 95-2613, July 1995.

⁶ Power, G. D., Cooper, G. K. and Sirbaugh, J. R., "NPARC 2.2 - Features and Capabilities," AIAA Paper 95-2609, July 1995.

⁷ Beam, R., and Warming, R.F., "An Implicit Finite Difference Algorithm for Hyperbolic Systems in Conservation Law Form," Journal of Computational Physics, vol. 22, no. 1, September 1976.

⁸ Jameson, A., Schmidt, W., and Turkel, E., "Numerical Solutions of the Euler Equations by Finite Volume Methods using Runge-Kutta Time Stepping Techniques," AIAA Paper 81-1259, June 1981.

⁹ Chien, K.-Y., "Predictions of Channel and Boundary-Layer Flows with a Low-Reynolds-Number Turbulence Model," AIAA Journal, vol. 20, no. 1, pp. 33-38, January 1982.

¹⁰ Wilcox, D.C., Turbulence Modeling for CFD, DCW Industries, Inc. La Canada, CA, 1993

¹¹ General Aerodynamic Simulation Program Version 3: User Manual, ISBN 0-9652780-0-X, Aerosoft Inc., Blacksburg, Virginia, 1996.

¹² Roe, P.L. "Approximate Riemann Solvers, Parameter Vectors and Difference Schemes," Journal of Computational Physics, vol. 43, pp. 357-372, October 1981.

¹³ Van Albada, G.D., Van Leer, B., and Roberts, W.W., "A Comparative Study of Computational Methods in Cosmic Gas Dynamics," Astronomy and Astrophysics, vol. 108, no. 1, pp. 76-84, April 1982.

¹⁴ Kang, S.-W., Dunn, M.G., and Jones, W.L., "Theoretical and Measured Electron Density distributions for the RAM Vehicle at High Altitudes," AIAA Paper 72-689, June 1972.

¹⁵ Billig, F.S., "Design and Development of Single-Stage-to-Orbit Vehicles," Johns Hopkins APL Technical Digest, vol. 11, nos. 3 and 4, pp. 336-352, 1990.

¹⁶ Riggins, D.W., and McClinton, C.R., "Analysis of Losses in Supersonic Mixing and Reacting Flows," AIAA Paper 91-2266, June 1991.

¹⁷ Heiser, W.H., and Pratt, D. T., Hypersonic Airbreathing Propulsion, American Institute of Aeronautics and Astronautics, Washington D.C., 1994.

	\mathbf{x}_{cl}/r_{cl}	\mathbf{r}_{cl}/r_{cl}	A	B	C	D
Cowl lip	-2.8192	1.0000				
Begin spline 1	-2.4192	1.0000	1.3146E-01	6.1873E-01	6.8555E-01	8.9863E-01
Begin spline 2	-1.3600	0.7800	-5.2929E-03	8.7712E-02	-1.6807E-10	6.0445E-01
Station 3	0.0000	0.6045				

a. Cowl

	\mathbf{x}_{cb}/r_{cl}	\mathbf{r}_{cb}/r_{cl}				
Spike tip	-6.1164	0.0000				
			\mathbf{r}_{arc}/r_{cl}	\mathbf{x}_{arc}/r_{cl}	\mathbf{y}_{arc}/r_{cl}	
Begin circular arc	-2.1040	0.8529	5.0000E-01	-2.0000E+00	3.6379E-01	
			A	B	C	D
Begin spline 3	-2.0000	0.8638	-1.4944E-02	-2.8465E-01	-9.5929E-01	-3.5726E-02
Begin spline 4	-1.3600	0.7498	1.1242E-01	4.8397E-01	3.7978E-01	6.5394E-01
Begin spline 5	-1.1100	0.6749	2.1372E-02	-2.6519E-03	-3.6397E-01	
Centerbody trailing edge	0.0000	0.3034				

b. Centerbody

Splines defined by,
$$\frac{r}{r_{cl}} = A \left(\frac{x}{r_{cl}} \right)^3 + B \left(\frac{x}{r_{cl}} \right)^2 + C \frac{x}{r_{cl}} + D$$

Table 1. Inlet geometry

M_0	Assumed M_1	$\Delta x/r_{c1}$	A_c/A_2
0.500	0.500	-0.604	3.665
0.800	0.800	-0.604	3.665
1.000	1.000	-0.604	3.665
1.500	1.500	-0.604	3.665
2.000	2.000	-0.604	3.665
2.500	2.500	-0.470	4.687
4.000	4.000	-0.272	8.309
6.000	5.933	-0.143	16.349
8.000	7.749	-0.143	16.349
10.000	9.395	-0.143	16.349
12.000	10.855	-0.143	16.349

Table 2. Centerbody spike translation schedule

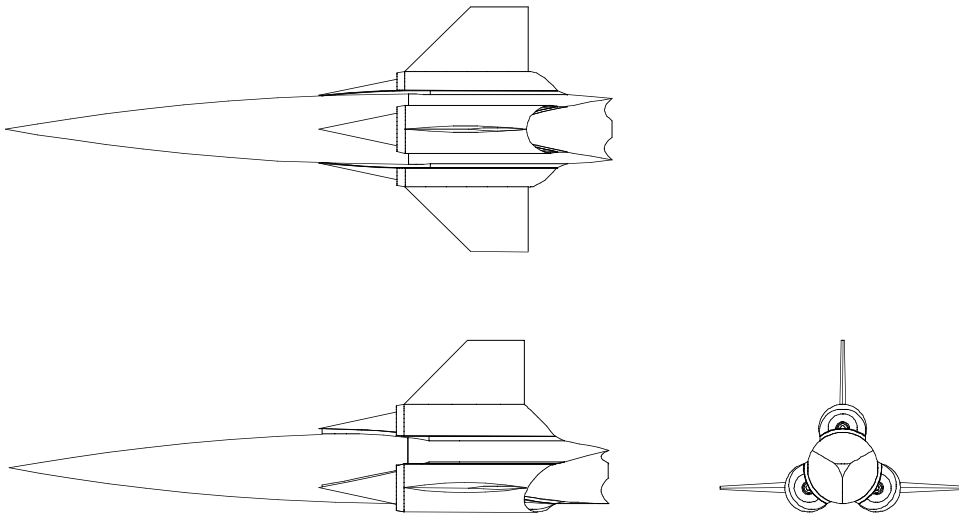


Figure 1. Trailblazer vehicle

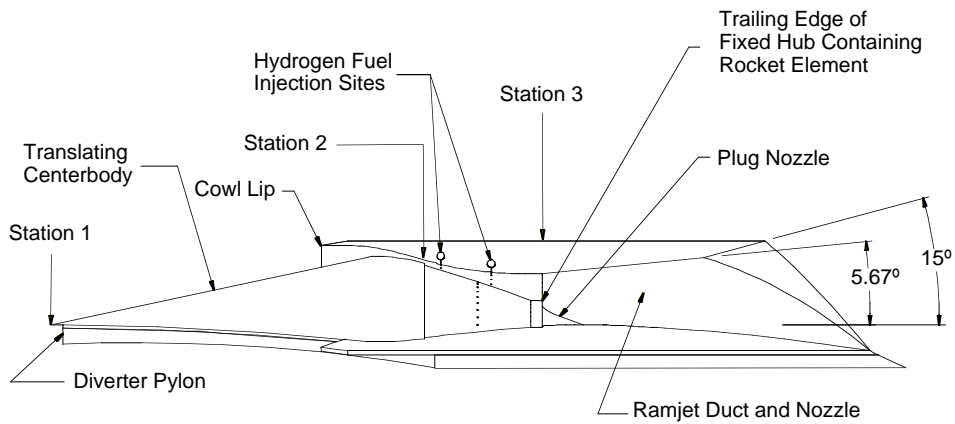


Figure 2. Trailblazer RBCC engine

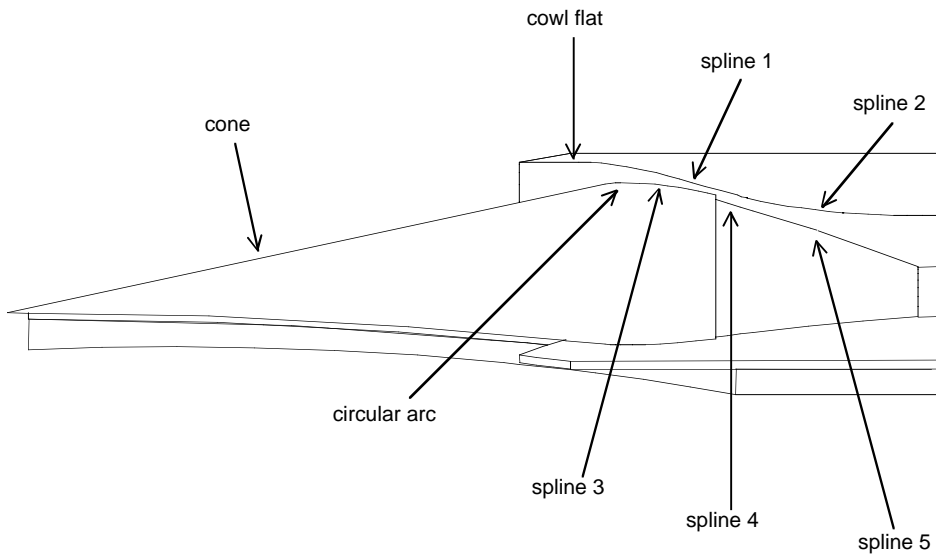
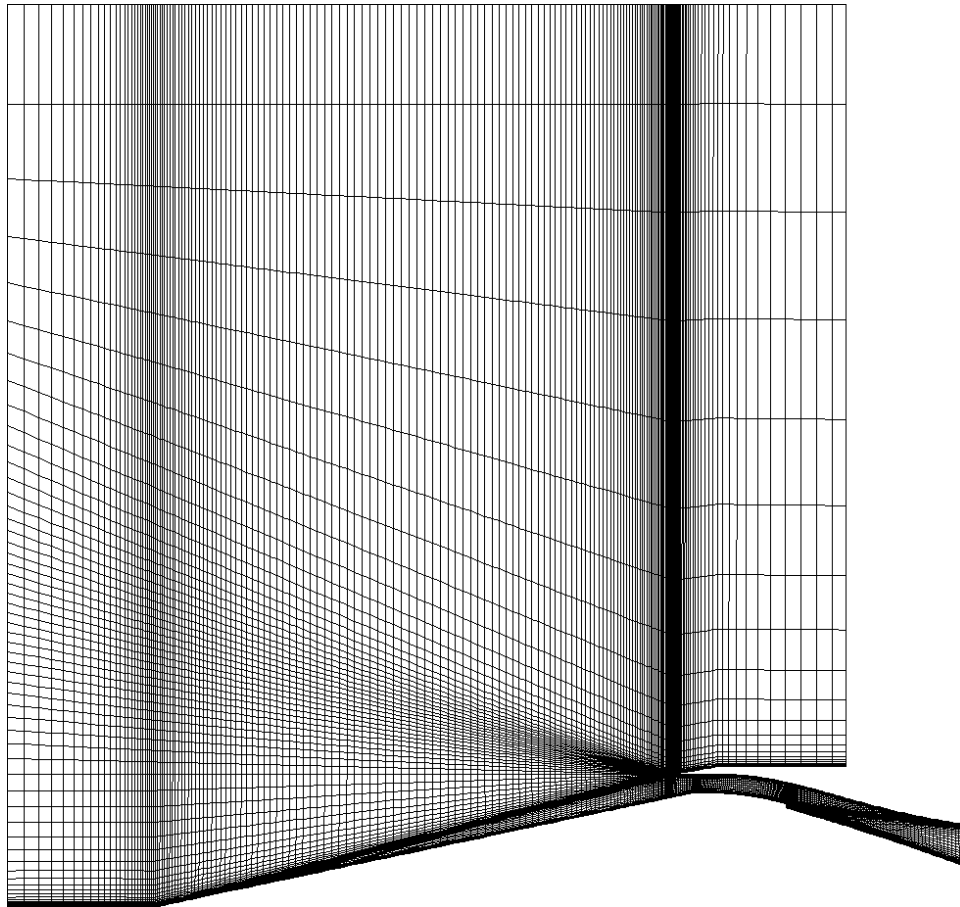
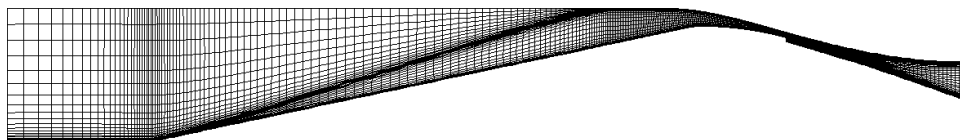


Figure 3. Inlet geometry definition



a. Full grid



b. Reduced grid for started supersonic cases

Figure 4. Computational grid

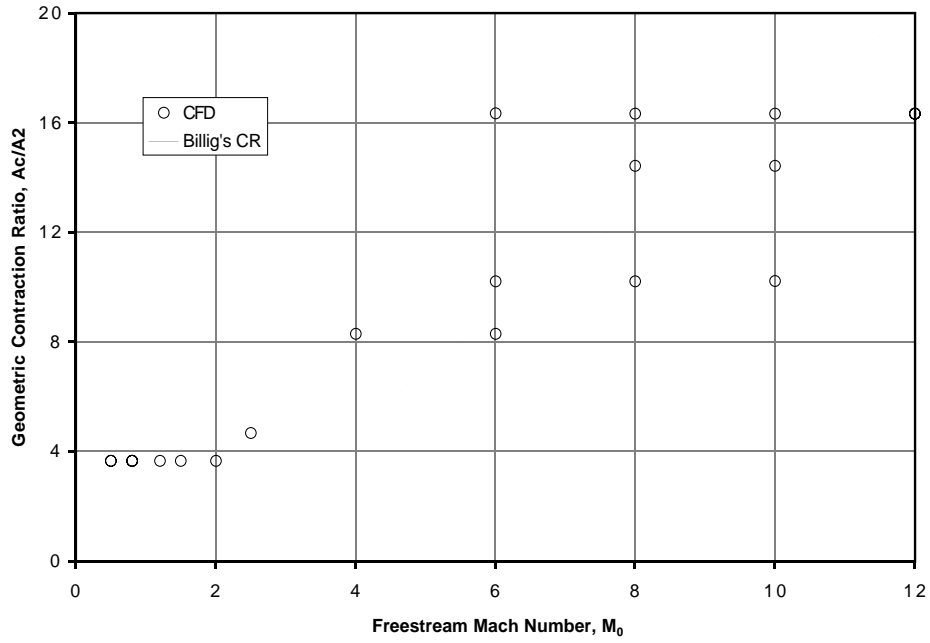
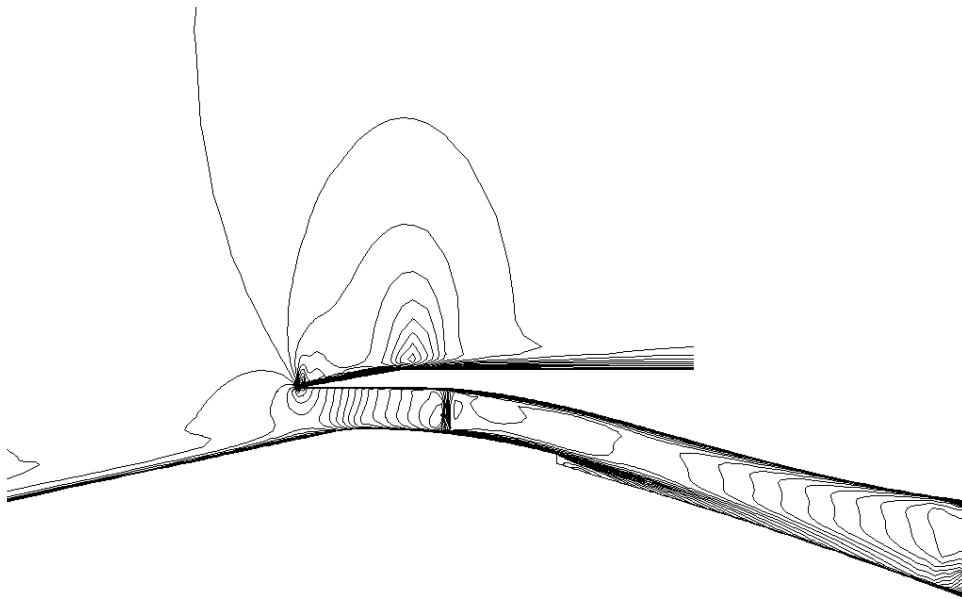
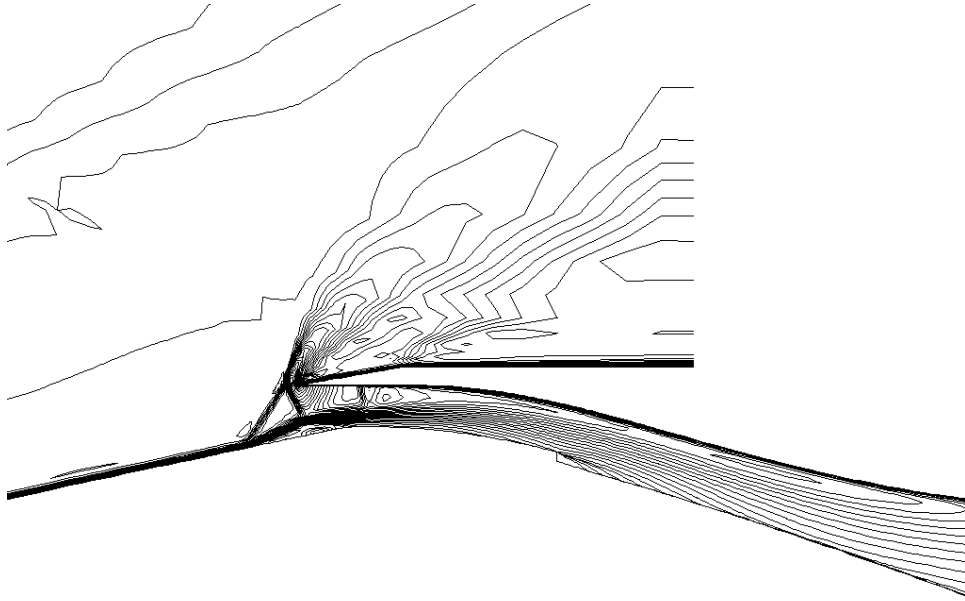


Figure 5. Contraction ratios analyzed



a. $M_0 = 0.8$

Figure 6. Mach number contours



b. $M_0 = 2$



c. $M_0 = 6$

Figure 6. Continued

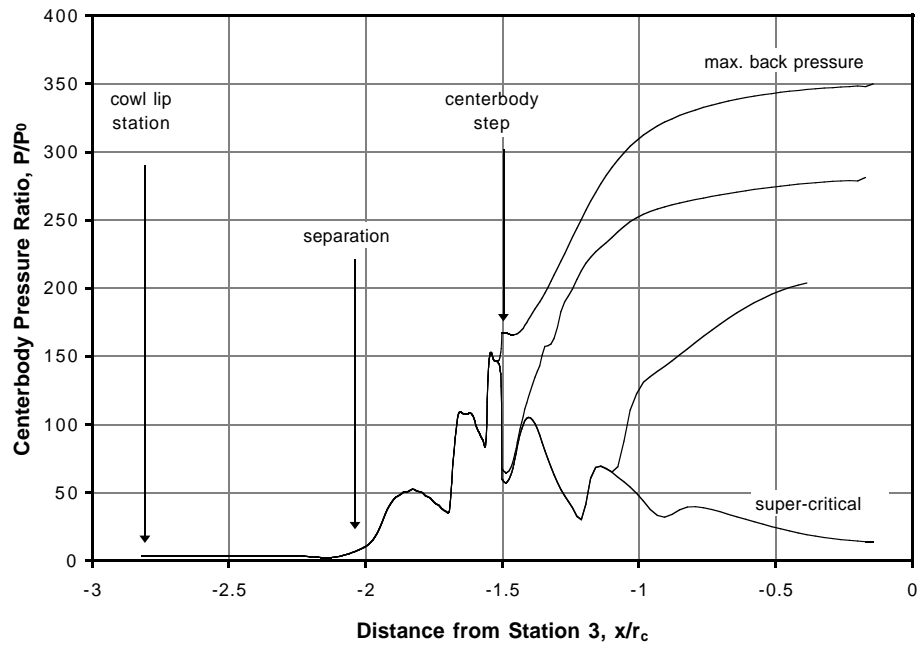


Figure 7. Centerbody pressure distributions, $M_0 = 6$

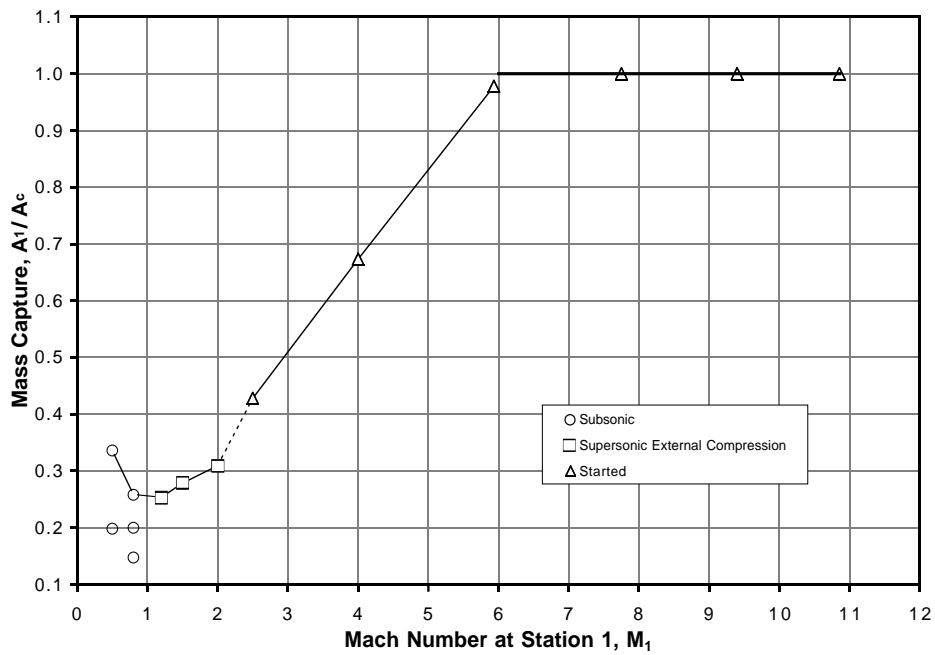


Figure 8. Inlet mass capture

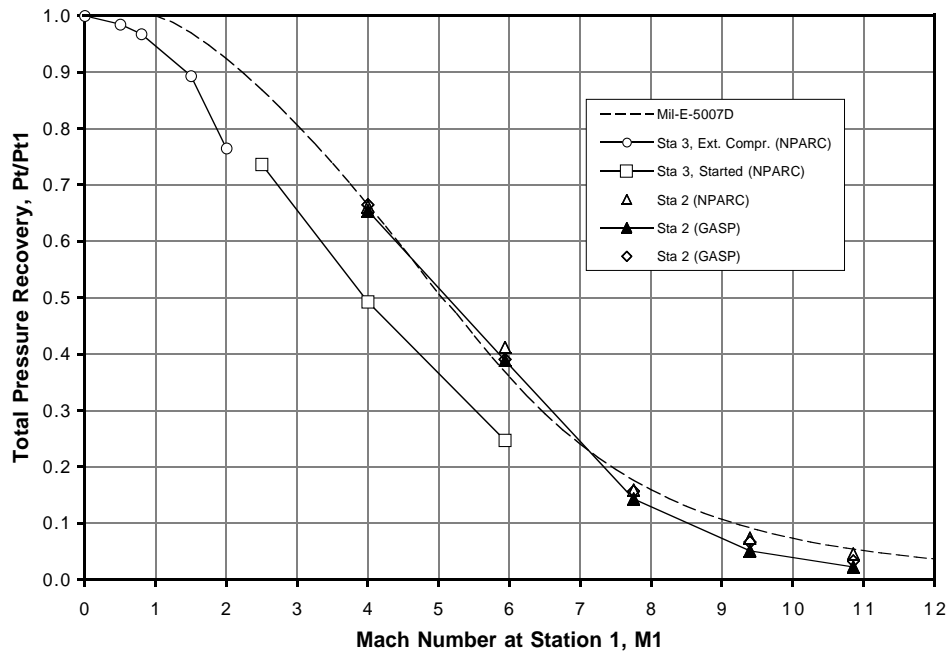


Figure 9. Inlet recovery

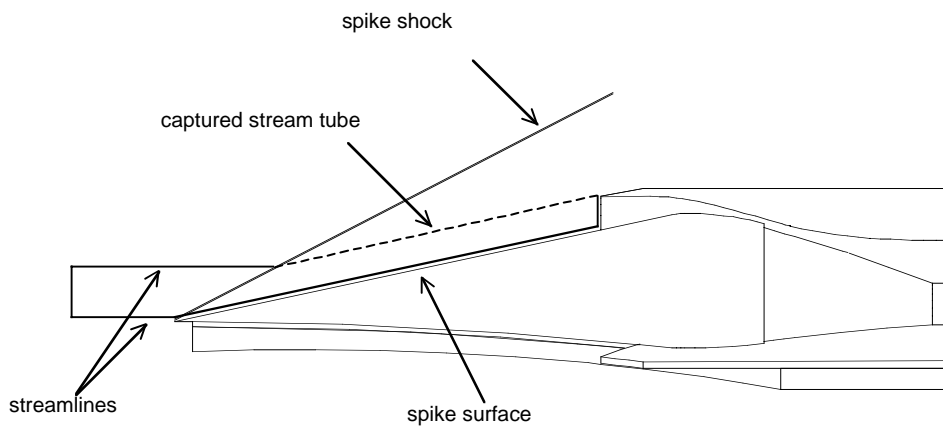


Figure 10. Control volume for drag calculation

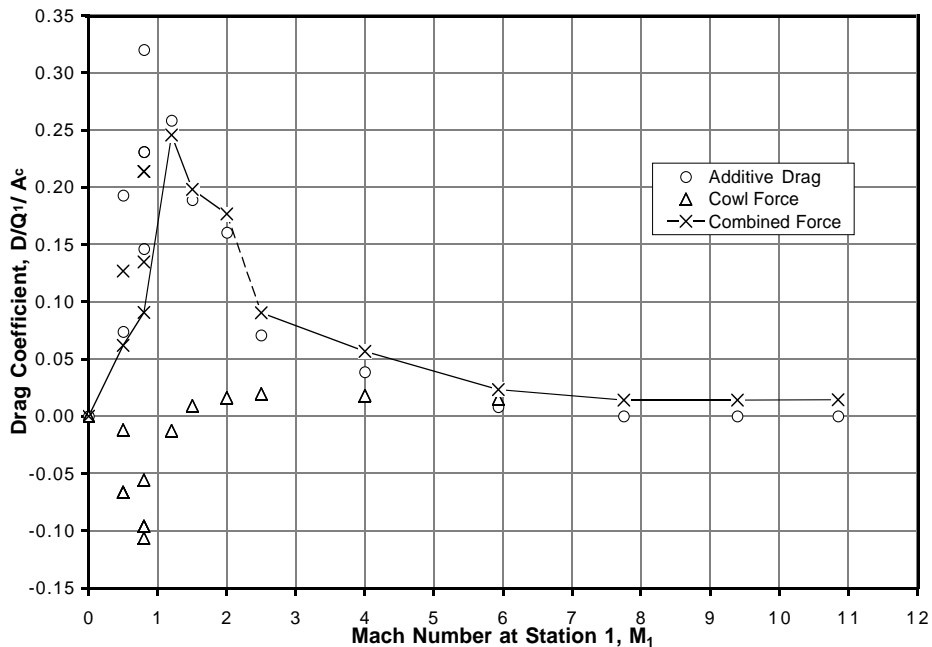


Figure 11. Inlet drag

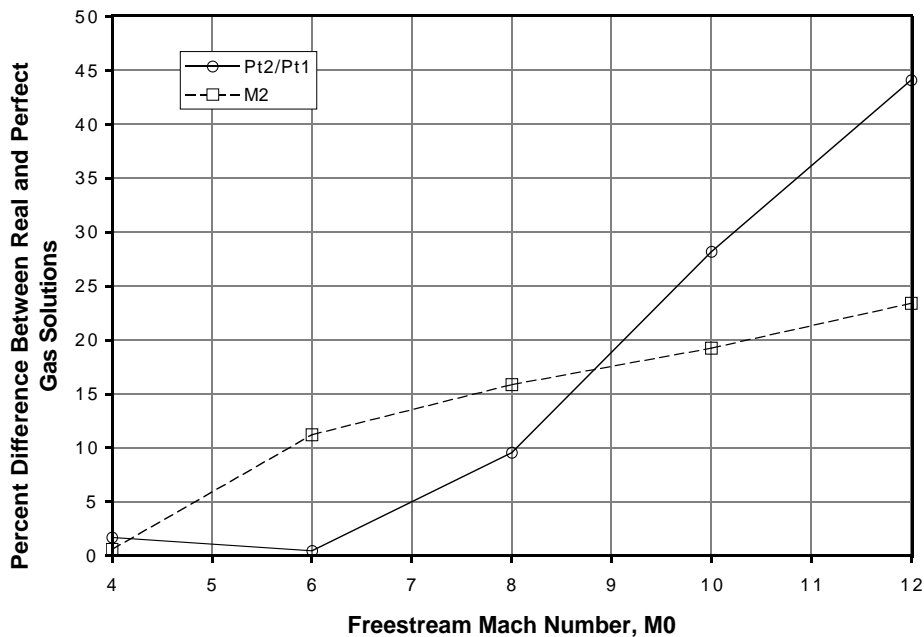


Figure 12. Percent difference between real and perfect gas recoveries and Mach number at station 2

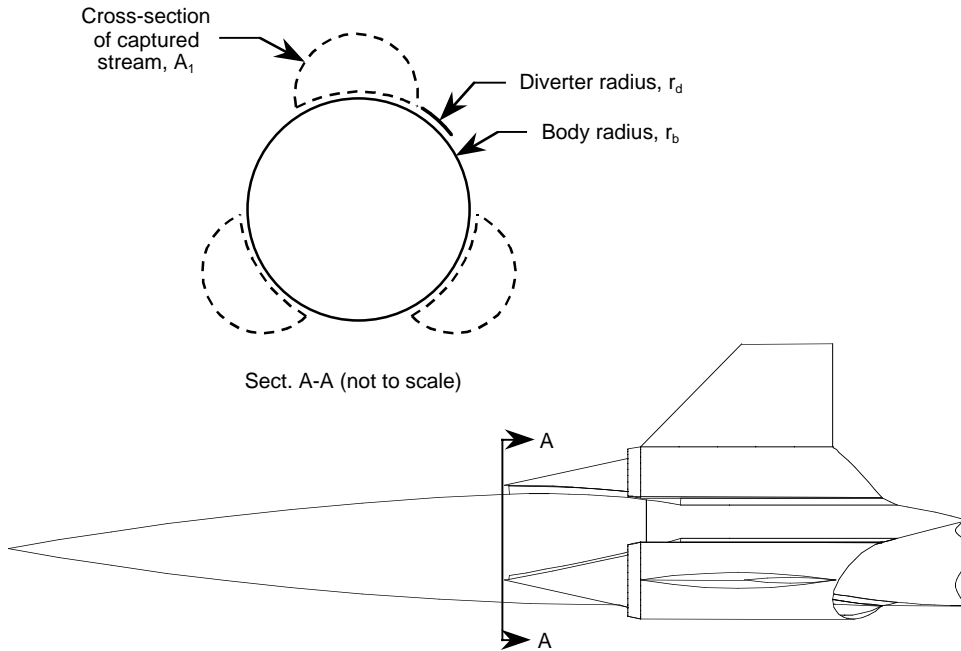


Figure 13. Projected capture area for precompression analysis

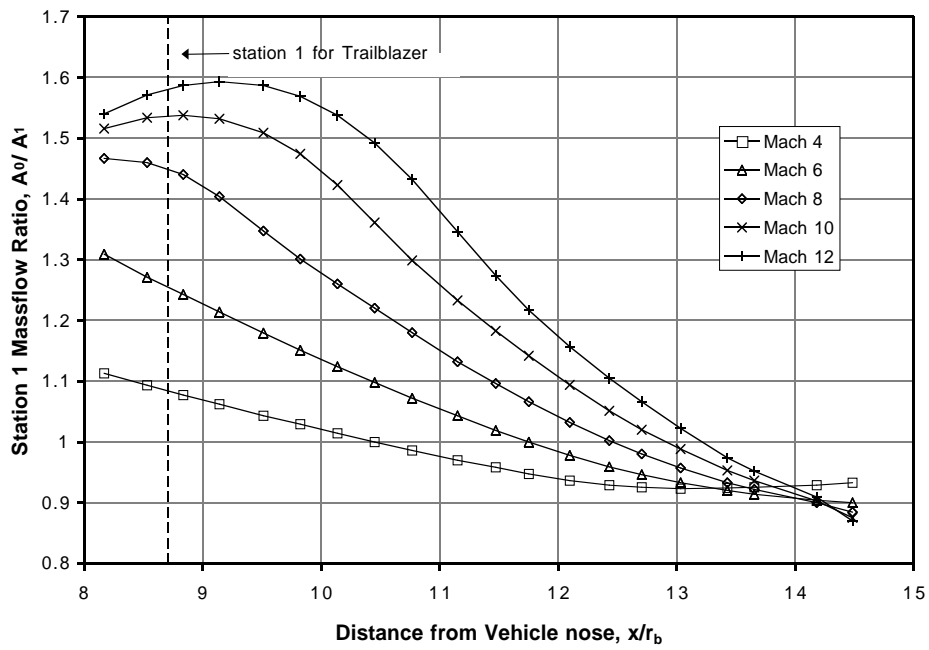
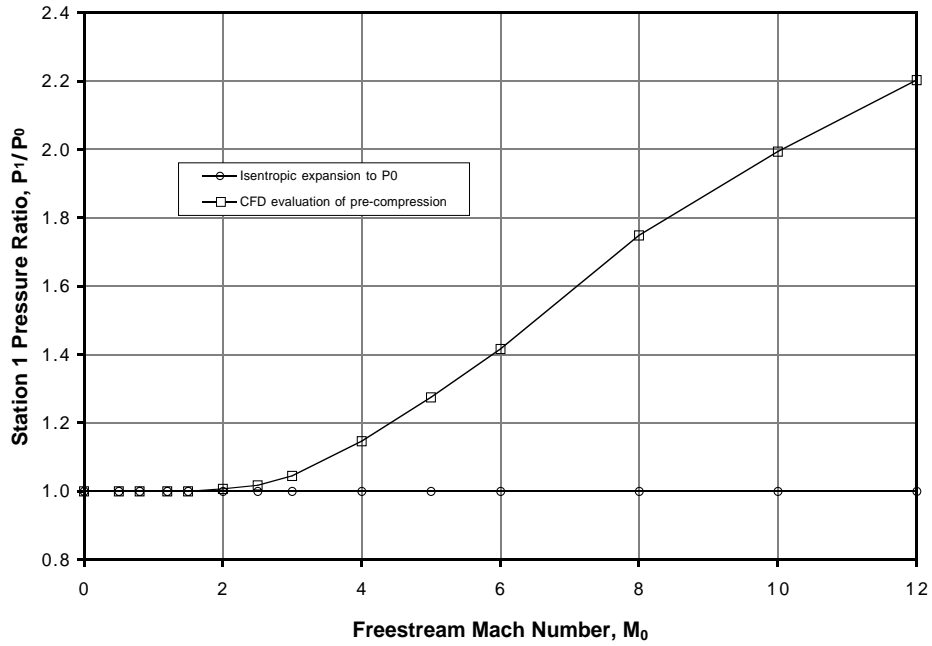
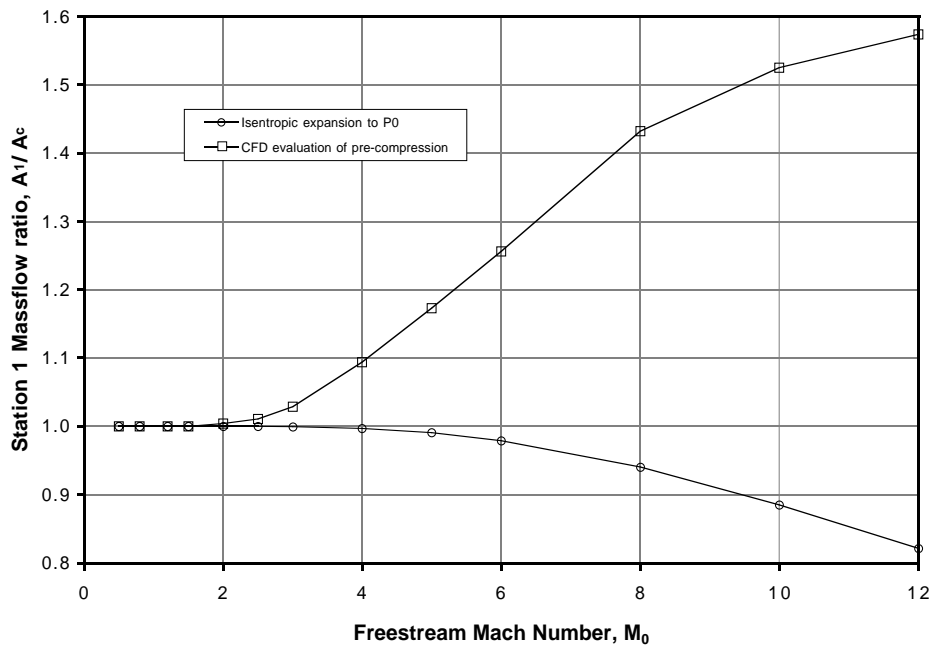


Figure 14. Variation of mass capture with station 1 location

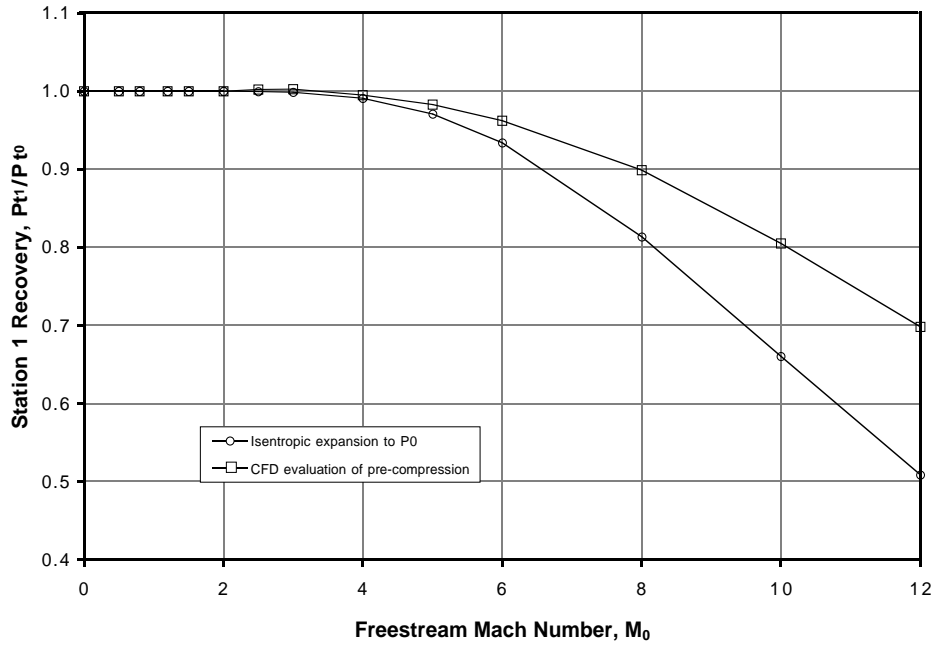


a. Pressure

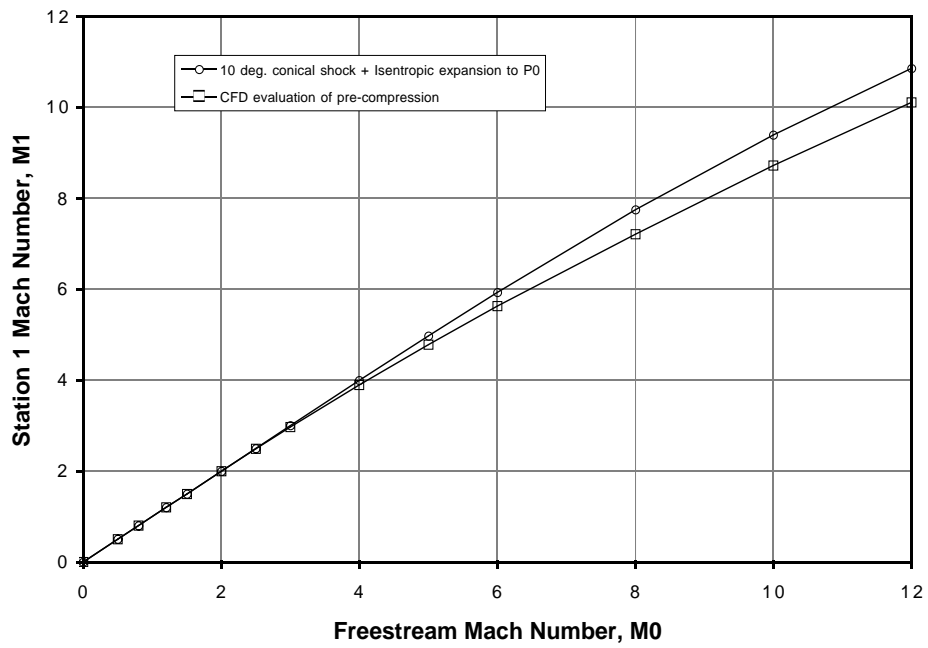


b. Mass capture

Figure 15. Effect of forebody compression



c. Recovery



d. Mach number

Figure 15. Continued

REPORT DOCUMENTATION PAGE			<i>Form Approved</i> <i>OMB No. 0704-0188</i>	
Public reporting burden for this collection of information is estimated to average 1 hour per response, including the time for reviewing instructions, searching existing data sources, gathering and maintaining the data needed, and completing and reviewing the collection of information. Send comments regarding this burden estimate or any other aspect of this collection of information, including suggestions for reducing this burden, to Washington Headquarters Services, Directorate for Information Operations and Reports, 1215 Jefferson Davis Highway, Suite 1204, Arlington, VA 22202-4302, and to the Office of Management and Budget, Paperwork Reduction Project (0704-0188), Washington, DC 20503.				
1. AGENCY USE ONLY (Leave blank)		2. REPORT DATE June 1999	3. REPORT TYPE AND DATES COVERED Technical Memorandum	
4. TITLE AND SUBTITLE Inlet Development for a Rocket Based Combined Cycle, Single Stage to Orbit Vehicle Using Computational Fluid Dynamics			5. FUNDING NUMBERS WU-523-61-13-00	
6. AUTHOR(S) J.R. DeBonis, C.J. Trefny, and C.J. Steffen, Jr.				
7. PERFORMING ORGANIZATION NAME(S) AND ADDRESS(ES) National Aeronautics and Space Administration John H. Glenn Research Center at Lewis Field Cleveland, Ohio 44135-3191			8. PERFORMING ORGANIZATION REPORT NUMBER E-11744	
9. SPONSORING/MONITORING AGENCY NAME(S) AND ADDRESS(ES) National Aeronautics and Space Administration Washington, DC 20546-0001			10. SPONSORING/MONITORING AGENCY REPORT NUMBER NASA TM-1999-209279 AIAA-99-2239	
11. SUPPLEMENTARY NOTES Prepared for the 35th Joint Propulsion Conference & Exhibit cosponsored by AIAA ASME, SAE, and ASEE, Los Angeles, California, June 20-24, 1999. Responsible person, J.R. DeBonis, organization code 5860, (216) 433-6581.				
12a. DISTRIBUTION/AVAILABILITY STATEMENT Unclassified - Unlimited Subject Categories: 02, 07, and 15 This publication is available from the NASA Center for AeroSpace Information, (301) 621-0390.			12b. DISTRIBUTION CODE	
13. ABSTRACT (Maximum 200 words) Design and analysis of the inlet for a rocket based combined cycle engine is discussed. Computational fluid dynamics was used in both the design and subsequent analysis. Reynolds averaged Navier-Stokes simulations were performed using both perfect gas and real gas assumptions. An inlet design that operates over the required Mach number range from 0 to 12 was produced. Performance data for cycle analysis was post processed using a stream thrust averaging technique. A detailed performance database for cycle analysis is presented. The effect of vehicle forebody compression on air capture is also examined.				
14. SUBJECT TERMS Air breathing engines; Computational fluid dynamics; Hypersonic inlets; Integral rocket ramjets			15. NUMBER OF PAGES 24	
			16. PRICE CODE A03	
17. SECURITY CLASSIFICATION OF REPORT Unclassified	18. SECURITY CLASSIFICATION OF THIS PAGE Unclassified	19. SECURITY CLASSIFICATION OF ABSTRACT Unclassified	20. LIMITATION OF ABSTRACT	